Non-Invasive Transdermal Delivery of Chemotherapeutic Molecules In Vivo Using Superparamagnetic Iron Oxide Nanoparticles

Vanisri Raviraj
The University of Sydney
Binh T.T. Pham
The University of Sydney
Nguyen T.H. Pham
The University of Sydney
Byung J. Kim
The University of Sydney
Lai F. Kok
Conde S. Januario Hospital
Nicole Painter
The University of Sydney
Naomi C. Delic
The University of Sydney
Stephen K. Jones
Zeta Therapeutics
Brian S. Hawkett
The University of Sydney
J. Guy Lyons (guy.lyons@sydney.edu.au)
Centenary Institute https://orcid.org/0000-0002-4835-4663

Research

Keywords: melanoma, transdermal, chemotherapy, nanoparticle, skin, doxorubicin, 5-fluorouracil

Posted Date: December 11th, 2020

DOI: https://doi.org/10.21203/rs.3.rs-118627/v1

Version of Record: A version of this preprint was published on February 6th, 2021. See the published version at https://doi.org/10.1186/s12645-021-00079-7.

Abstract

Background: The skin is both a target and a potential conduit for the delivery of drugs, but its cornified cell layer resists penetration by most molecules. This study investigated the potential of superparamagnetic iron oxide nanoparticles to facilitate the transdermal delivery of anti-cancer agents.

Results: Chemotherapeutic cancer drugs were applied with or without nanoparticles to the skin of hairless mice, and their ability to penetrate the skin was assessed using fluorescence microscopy and tumor growth. Nanoparticles enhanced the penetration of the skin by doxorubicin and 5-fluorouracil as determined by fluorescence microscopy and growth retardation of experimental melanoma in immunocompetent, syngeneic mice. This drug enhancement did not require conjugation or encapsulation of the drugs by the nanoparticles – simple co-administration sufficed. Nanoparticles applied topically to melanomas increased the cytotoxicity and immune cell infiltration induced by co-administered 5-fluorouracil, and also reduced vascularization of the tumors independently of 5-fluorouracil.

Conclusion: Correctly formulated superparamagnetic iron oxide nanoparticles can facilitate the chemotherapeutic effectiveness of cytotoxic drugs on skin tumors by both increasing their transdermal penetration and ameliorating host-tumor interactions. This enhancement of skin penetration occurs without the need for conjugation or encapsulation of the co-administered drugs and so will likely be applicable to other drugs, also.

Background

Delivery of therapeutic molecules through the skin has recently gained much scientific attention as a direct and efficient conduit for treating diseases, due to the skin's size and accessibility (Gautam et al. 2016). Transdermal delivery systems have several advantages over other methods: they are non-invasive, needle-free and the drugs can be delivered in a controlled manner that increases systemic bioavailability while bypassing metabolism in the liver (Prausnitz and Langer 2008; Alkilani et al. 2015; Palmer and DeLouise 2016). In the case of skin diseases, transdermal delivery can enable local concentrations of drugs to achieve therapeutic levels while keeping the systemic level very low, thereby reducing off-target toxicity. However, delivery of therapeutic molecules through the skin poses particular challenges. In particular, the stratum corneum (SC) is impermeable to almost all compounds larger than 500 Da (Matsui and Amagai 2015).

The past two decades have seen the development of techniques to improve the penetration of drugs through the skin, including iontophoresis (Cazares-Delgadillo et al. 2007), sonophoresis (Alvarez-Roman et al. 2003), electroporation (Lombry et al. 2000), microneedles (Prausnitz 2004), magnetophoresis (Murthy et al. 2010), microdermabrasion (Herndon et al. 2004) and electron beam irradiation (Kotiyan and Majali A., Vavia P, Bhardwaj Y, Sabarwal S 2004). However, the undesirable side effects of these techniques include skin irritation, pain and potential for infection.

Nanoparticles have the potential to significantly improve the penetration of large molecules across the SC, thereby improving bioavailability without compromising the skin barrier to pathogenic microbes. They can offer stability, biodegradability, low toxicity, and biocompatibility (Dianzani et al. 2014; Wang et al. 2016; Pelaz et al. 2017; Carter et al. 2019). Larger nanoparticles (20–30 nm) can penetrate only through hair follicles (Zvyagin et al. 2008), limiting their usefulness for transdermal applications. In contrast, nanoparticles smaller than 10 nm can permeate through both the SC and hair follicles (Hansen and Lehr 2012). However, aggregation of small nanoparticles in vivo can limit their tissue penetration and increase toxicity (Pelaz et al. 2017). The surface charge of nanoparticles also affects their ability to penetrate the skin.

Melanoma is the most aggressive common skin cancer with a 5-year survival rate of 10% among metastatic melanoma patients (Garbe et al. 2011; Mundra et al. 2015). In recent years, immunotherapies and chemotherapies targeted to specific mutant proteins have revolutionised the therapy of melanoma, but lack of response and relapse through resistance are common and so conventional cytotoxic chemotherapies still play a major role in its management (Tang et al. 2017; Vanella et al. 2019). Several chemotherapeutic drugs are available for melanoma treatment, including dacarbazine, temozolomide, 5-fluorouracil (5-FU), paclitaxel and platinum compounds. However, the overall response rate is less than 20% and each of these agents produces unwanted systemic side effects. Applications of nanoparticles to the treatment of melanoma is of growing interest (Tang et al. 2017), despite the aforementioned drawbacks of size, charge and aggregation inherent in many nanoparticles. Carbon nanotubes loaded with doxorubicin (DOX) induced melanoma cell death *in vitro* and abrogated tumor growth in xenograft mouse models (Chaudhuri et al. 2010). Inorganic nanoparticles based on silica and aluminium (Oh et al. 2012; Yu et al. 2013), protein-based nanoparticles (Vannucci et al. 2012) and DOX-loaded liposomes (Lohade et al. 2016) have also been investigated for melanoma treatment.

Superparamagnetic iron oxide nanoparticles (SPIONs) have been successfully used in various biomedical applications that benefit from their magnetic properties, biocompatibility, low toxicity, easy separation methodology and flexibility of surface modification (Shubayev et al. 2009; Veiseh et al. 2010; Kievit et al. 2011; Hasany et al. 2012; Ali et al. 2016; Palanisamy and Wang 2019). However, to date, no SPIONs have been commercialized successfully for drug delivery purposes. We have developed a unique coating technology for SPIONs that produces a highly stable dispersion for biomedical applications (Jain et al. 2010; Eamegdool et al. 2014; Pham et al. 2015, 2017). These SPIONs are non-toxic *in vitro* and *in vivo* and can be readily tailored to have different coating compositions and functional groups at the end of stabilizers (Bryce et al. 2013; Eamegdool et al. 2014; Pham et al. 2018). We have shown that co-administration of our nanoparticles with a cytotoxic drug can enhance the penetration of the drug in an *in vitro* spheroid model (Bryce et al. 2013).

In this study, we investigated the potential of our sterically stabilised SPIONs as chemotherapy adjuvants in transdermal drug delivery *in vivo*. We found that topical co-administration of these SPIONs improved transdermal delivery and the anti-tumor responses of mouse melanomas to chemotherapeutic drugs.

Methods

Reagents

Reversible addition-fragmentation chain-transfer (RAFT) agents 2-[(butylsulfanyl)carbonothioyl]sulfanyl propanoic acid (C_4-RAFT) and methoxy-polyethylene glycol modified 2-[(butylsulfanyl)carbonothioyl] sulfanyl propanoic acid were kindly provided by Dr Algi Serelis (DuluxGroup). Fe(II) chloride tetrahydrate (99%), Fe(III) chloride hexahydrate (98%), Fe(III) nitrate nonahydrate (99%), acrylamide (> 98%), rhodamine B isothiocyanate (> 70%), DOX (> 98%) and nitric acid (HNO_3, 65%, Suprapur®, Millipore) were purchased from Sigma-Aldrich (St. Louis, USA). Ammonium hydroxide (28% NH_3 in water) and sodium hydroxide (NaOH) (> 98%) were obtained from Ajax Finechem (Australia). 1,4-Dioxane (Fluka-Sigma-Aldrich, St Louis, USA), monoacryloxyethyl phosphate (MAEP, > 98%, PolySciences, Warrington, USA) and 4,4-azobis(4-cyanovaleric acid) (Wako, USA) were used as received.

Nanoparticles

Maghemite nanoparticles (γ-Fe_2O_3, average 25 nm core diameter, unless stated otherwise) were synthesized by the coprecipitation method (Massart et al. 1995) and sterically stabilized with a mixture of 90% poly(ethylene glycol) methyl ether (MPEG)-end and 10% NH_2-end macro-RAFT copolymers, prepared using RAFT polymerization (Pham et al. 2018). The polymers each contain a block of 10 units of MAEP to anchor MPEG or polyacrylamide to the SPIONs' surface, and either a block of 40 units of acrylamide and 17 units of poly(ethylene glycol) (PEG) (in MPEG-end-copolymer) or a block of 60 units of acrylamide (in NH_2-end-copolymer) for steric stabilization. We refer to these copolymer-coated nanoparticles as "10%NH_2-SPIONs". Transmission electron microscopy images were obtained using a JEOL 1400 microscope. Hydrodynamic diameter was measured by dynamic light scattering (DLS) using Malvern's Zetasizer nano ZS. The polymer content was 13% (w/w) of the dried solid as analysed by thermogravimetric analysis (Supplementary Fig. 1d). Iron concentration of the SPIONs was determined by flame atomic absorption spectroscopy (Varian AA800 spectrometer). For *in vivo* studies, 10%NH_2-SPIONs were dispersed in PBS to the final concentration of 5 mg/mL as Fe and then filtered through a 0.22 μm sterile syringe filter.

Rho-SPIONs were made by labelling 10%NH_2-SPIONs with rhodamine B isothiocyanate in PBS at room temperature in the dark for 4 hours. Free rhodamine was removed using Amicon Ultra MWCO 3000 centrifugation filter units. Fluorescence intensity of Rho-SPIONs was measured with a RF-5301 PC spectrofluorophotometer (Shimadzu, Kyoto, Japan).

Cell culture

Amelanotic tyrosinase-knockout B16-F10 melanoma cells were kindly provided by Dr Shweta Tikoo from the Centenary Institute, Sydney, Australia, and maintained in Advanced Dulbecco's modified Eagle's medium and 5% fetal bovine serum (Thermo Fisher Scientific, Waltham, USA). They were stably transfected with CEFLP-tdTomato-H2B eukaryotic expression plasmids using GenePORTER®3000

(Genlantis, San Diego, CA, USA). Transfected cells were selected with puromycin (10 µg/mL) and tdTomato-expressing cells were purified by flow cytometry on a BD Influx Cell Sorter.

Animals

A colony of hairless albino C57BL/6 mice was established from a breeding pair obtained from the Jackson Laboratory (strain 017840) and maintained by breeding homozygous males (Hr -/-) with heterozygous (Hr+/-) females. Mice were housed with dust-free bedding (Able Scientific, Australia), regular chow, water, environmental enrichment and 12 hour/12 hour light/dark cycles.

Transdermal delivery of SPIONs and chemotherapeutic drugs

Mice were anesthetised by intraperitoneal injection of ketamine (75 mg/kg) and medetomidine (1 mg/kg), placed on a warming pad and the back skin of the mice was cleaned with a 70% isopropyl alcohol swab (Livingstone International, Australia). Rho-SPIONs (20 µl of 2 mg/mL in PBS) were applied to the skin and left for 1 hour, after which excess liquid was wiped off with a wet cotton bud. PBS only (20 µL) was used for the control mouse. For chemotherapeutic drug delivery, a 30 µL mixture in PBS containing either both 10%NH_2-SPIONs (1.3 mg/mL as Fe) and DOX (0.17 mM), 10%NH_2-SPIONs only (1.3 mg/mL as Fe), or DOX only (0.17 mM), was applied to the mouse skin and then left for 1–2 hours, at which time unabsorbed material was removed by wiping. Anaesthesia was reversed with atipamezole (0.2 mg/kg).

The mice were imaged under anesthesia on a Carestream In-Vivo FX PRO (Carestream Health, Woodbridge, USA) using 550 nm excitation and 600 nm emission wavelength filters before application and 1, 2, 24 and 48 hours after application. They were then euthanized, and treated skins were fixed in 4% paraformaldehyde (PFA) overnight at 4^{o}C for fluorescent imaging.

In vivo melanoma model

Eight-week-old hairless albino C57BL/6 mice were injected subcutaneously with 1×10^4 B16F10-tdTomato amelanotic melanoma cells. Three days post injection, the mice were randomized into different treatment groups. Each group was topically treated at the tumor site 3 times/week with 60 µL of either vehicle (0.9% saline), 5-FU (1 mM) alone, 10%NH_2-SPIONs (1 mg/mL) alone, or a mixture of 5-FU (1 mM) and 10%NH_2-SPIONs (1 mg/mL). Tumor growth was measured using calipers and micrographs taken with a Dino-Lite AM4515ZT Edge Handheld Microscope. Tumor volume was calculated by the modified ellipsoidal formula (Tomayko and Reynolds 1989). Mice were euthanized when tumors reached 1 cm^3, or skin ulceration appeared to be imminent.

Histology and imaging

PFA-fixed skin samples from Rho-SPION-treated mice were embedded in Tissue-Tek® OCT (Sakura, Torrenace, CA), frozen and cut into 7 µm-thick sections. Sections were counterstained with 1 µg/mL for 5 minutes 4',6-diamidino-2-phenylindole (DAPI) (Sigma-Aldrich, St Louis, MO, USA), washed 3 times with PBS, mounted in Prolong Gold® anti-fade mounting media (Life Technologies, Carlsbad, CA) and cover-

slipped. Skin sections were stained with F4/80 primary antibody (1:200, SC-52664, BM8 clone, Santa Cruz Biotechnology, Dallas, USA) and goat anti-rat IgG (H + L) Alexa Fluor 488-for secondary Antibody (1:200, A-11006, ThermoFisher Scientific, Australia) to detect macrophage distribution in the skin. Images were acquired using an Olympus FV1000 confocal microscope (Olympus, Japan) and Leica SP5 and SP8 confocal microscopes (Leica Biosystem, Wetzlar, Germany).

B16-F10 melanoma tumors were fixed in 4% PFA overnight, embedded in paraffin, and cut into 4 μm-thick sections for hematoxylin and eosin (H&E) staining. The sections were deparaffinized, rehydrated and then incubated in an antigen retrieval solution (RD913M, pH 6.0, Pacheco, USA) for 20 min over a boiling water bath to retrieve antigen. Endogenous peroxidase activity was blocked using 0.3% (w/v) hydrogen peroxide. Sections were incubated for 1 hour at room temperature with antibodies: 1:25 anti-F4/80 monoclonal rat antibody (SC-52664, Santa Cruz Biotechnology, Dallas, USA) or the rat IgG2a isotype control (559073, R35-95 clone, BD Biosciences, North Ryde, Australia) and 1:75 anti-CD31 monoclonal rabbit antibody (77699T, D8V9E clone, Cell Signaling Technology, Danvers, USA) or the rabbit IgG isotype control (ab172730, EPR25A clone, Abcam, Melbourne, Australia). Detection was with Rat-on-Mouse HRP-Polymer, Biocare Medical (Pacheco, USA) or anti-rabbit EnVision + system HRP-polymer, and diaminobenzidine as substrate (Dako-Agilent, Santa Clara, USA). Slides were counterstained with Mayer's haematoxylin.

Image analysis

Cell morphology of H&E stained sections were characterised by the pathologist (LFK) to assess tumor borders and areas of tumor tissue necrosis. The pathologist was blinded to the treatments the specimens had received. Three mice per group were used for analysis and 4–6 regions were selected randomly in each tumor. Necrosis and whole tumor areas were measured using ImageJ software, and the percentage of the necrotic region was calculated by the total tumor area. Tumor-infiltrating lymphocytes were identified by a small cytoplasm:nucleus ratio, an oval, dark stained nucleus and a cell diameter of 7–10 μm and were counted manually using ImageJ.

The vascular area was quantified from CD31-stained images in which the diaminobenzidine signal had been segmented by spectral deconvolution (Ruifrok and Johnston 2001) and thresholded using Fiji image analysis software. The image representing CD31 staining was then binarized and holes (vascular lumens) were filled. The CD31-positive stained area and total tumor area were measured in each tumor section, from which the percentage of CD31 stained area was calculated.

Statistical analyses were done using GraphPad Prism v. 8.4.

Results

SPIONs penetrate mouse skin

SPIONs were synthesized from maghemite particles by coating them with polyacrylamide and PEG copolymers, 10% of which were NH_2-end derivatised for steric stabilization (Suppl. Figure 1a). The particles had a core diameter of 20–30 nm, a hydrodynamic diameter of 72 nm, a polymer content of 13% w/w, a polydispersity index of 0.11 and a zeta potential of -40 mV (Suppl. Figure 1b-e). To evaluate the penetration of SPIONs into mouse skin, fluorescent rhodamine-labelled SPIONs (Rho-SPIONs) (Suppl. Figure 1f) were topically applied to hairless albino C57BL/6 mice. Live-mouse images (Fig. 1a, Suppl. Figure 2,3) show a strong rhodamine fluorescent signal on the mouse's skin after one hour of application. After 24 hours, the signal intensity of the Rho-SPIONs was lower and dispersed over a larger area. No fluorescent signal above autofluorescence was detected on the control mouse. Fluorescence microscopy of fixed skin from the application areas of Rho-SPION-treated mice show that SPION particles penetrated through the SC within 24 hours of application, accumulating most strongly in the epidermis, but also penetrating and being retained throughout the dermis (Fig. 1b, Suppl. Figure 3).

SPIONs improve the transdermal penetration of doxorubicin

To test whether topical application of SPIONs enhances the penetration of chemotherapy drugs into the skin, we topically applied the chemotherapeutic DNA intercalating drug, doxorubicin (DOX, molecular mass 544), with and without SPIONs to the skin of the dorsal back and ear. The fluorescent properties of DOX enabled microscopic and macroscopic visualization of drug penetration into the mouse skin.

Live-mouse imaging 2 hours after topical application showed strong DOX fluorescence in the application area for DOX applied with or without SPIONs, which decreased after 24 and 48 hours (Fig. 2a). Macroscopically, the DOX signal was higher in the area treated with DOX alone compared with the area treated with both DOX and SPIONs at 2 hours, 24 hours and 48 hours after application. Confocal microscopy of cryosections of fixed tissue was used to determine the extent of penetration of DOX into the skin (Fig. 2b, Suppl. Figure 4). Mice treated with DOX alone showed poor penetration of DOX into the skin whereas mice treated with both DOX and SPIONs showed a strong DOX signal within the epidermis that extended into the dermis. It should be noted that DOX remaining on the surface of the epidermis would not have intercalated into cell DNA and therefore may have been lost during the fixation and counterstaining process; this would explain why there is no DOX signal detected in the DOX + PBS cryosections despite a strong signal being observed at the application site in the whole animal images.

Co-application with SPIONs improves the response of melanoma tumors to 5-FU

5-FU is a hydrophilic, negatively charged molecule that cannot easily penetrate through the hydrophobic, negatively charged SC (Fang et al. 2004). To determine whether SPIONs could improve the response to transdermal treatment by 5-FU, we topically treated subcutaneous B16-F10 melanoma tumors in the skin of mice with 5-FU and/or SPIONs, starting three days post-tumor cell inoculation, then 3 times per week until mice were euthanized. Comparing the growth curves up to day 17, the latest point at which all mice survived, 5-FU on its own appeared to slightly accelerate tumor growth compared with saline (Fig. 3a), but this effect did not reach statistical significance ($p = 0.52$ by repeated measures ANOVA). Topical

application of 5-FU with SPIONs significantly reduced tumor growth compared with topical application of 5-FU alone ($p = 0.0072$), but SPIONs alone did not ($p = 0.96$). Furthermore, topical co-application of 5-FU with SPIONs significantly improved the survival of mice (i.e. the time for the tumor to reach 1 cm diameter, the ethical endpoint; Fig. 3bB) when compared with 5-FU alone ($p = 0.012$, log-rank test).

To determine whether the reduced growth of melanoma tumors in the SPION/5-FU co-administration group was due to an enhanced cytotoxicity, we examined tumors histologically for necrosis. Photomicrographs showed more pronounced necrosis in tumors treated topically with 5-FU + SPIONs than in those treated with 5-FU alone, SPIONs alone or saline vehicle control (Fig. 4a). Quantification by image analysis confirmed that this pro-necrotic effect was statistically significant ($p = 0.040$ and $p = 0.026$, respectively, by one-way ANOVA with Sidak's multiple comparisons correction) (Fig. 4b). Moreover, combined 5-FU + SPION topical treatment increased the infiltration of tumors by both lymphocytes (Fig. 5a) and macrophages (Fig. 5b), and reduced their vascularization (Fig. 5c) compared with tumors treated topically with 5-FU alone or saline control. Interestingly, SPIONs alone were able to increase lymphocyte and macrophage infiltration and reduce vascularization (Fig. 5a-c). Thus, similar to the DOX studies, co-administration of SPIONs facilitated the transdermal effects of 5-FU.

Discussion

There has been a limited number of reports investigating the permeability of inorganic nanoparticles through the skin, with or without conjugated drugs (Baroli et al. 2007; Nose et al. 2012; Anandhakumar and Raichur 2013; Fernandes et al. 2015; Santini et al. 2015; Hsiao et al. 2016; Ozcan et al. 2020). Most previous transdermal nanoparticle studies focused on gold nanoparticles, with studies investigating Fe_3O_4 magnetic nanoparticles for topical application rare (Baroli et al. 2007; Rao et al. 2015; Santini et al. 2015). In this study, the excellent penetration of our SPIONs through the skin might be explained by their steric stabilizers, which prevent the particles from aggregating and accumulating on the skin surface. In addition, NH_2 end groups on the coating layer are protonated at low pH which might facilitate their penetration of the SC.

DOX has been used on its own or in combination with other agents against many cancers, including melanoma, lung, breast and ovarian cancer (Weiss 1992; Pan et al. 2019). However, there are two main concerns of DOX: cardiotoxicity and poor penetration into a solid tumor. To overcome these limitations, the first nano-based, PEGylated liposomal DOX was approved for the treatment of ovarian cancer and Kaposi's sarcoma (Barenholz 2012). Since then, several nanoparticle formulations conjugated or loaded with have DOX been developed for use in cancers (Wang et al. 2011; Chen et al. 2015; Lv et al. 2017; Sheth et al. 2020). However, nanoparticles conjugated or loaded with chemotherapy drugs may be susceptible to inefficient release of drugs at the target site, which is avoided by our adjuvant approach (Bryce et al. 2013). We previously showed that co-administration of 10%NH_2-SPIONs with DOX increased drug penetration into cancer cell spheroids compared with DOX alone (Bryce et al. 2013). The results in this study confirm that co-administration of SPIONs additionally enhances the penetration and bioactivity of DOX and 5-FU through the SC and epidermal layers into the dermal layer of the skin of a living animal,

without the need for covalently binding DOX to the nanoparticles. The range of molecules whose transdermal penetration is enhanced by these SPIONs without covalent attachment remains to be determined, but conceivably could include other anticancer and immunomodulatory drugs.

For many years, the infiltration of tumors by lymphocytes has been used as a measure of treatment success in clinical trials for melanoma treatment (Rosenberg et al. 1994) and numerous reports indicate that tumor infiltrating lymphocytes play an essential role in mediating response to chemotherapy in many cancers (Galluzzi et al. 2015). In this study, we showed that SPIONs applied topically to a skin melanoma can enhance the cytotoxicity of 5-FU, increasing necrosis and slowing tumor growth. The increased necrosis may be a combination of enhancing the penetration of 5-FU, increasing leukocye infiltration and reducing the vascularity of the tumors. The effects of SPIONs on tumor vascularization and immune cell infiltration are independent of 5-FU. A recent study on magnetically localized polyethyleneimine-coated SPIONs also found an enhancement of macrophage infiltration and reduced vascularization of tumors in the absence of cytotoxic drugs (Mulens-Arias et al. 2019), but did not examine the effect of SPIONs on drug delivery.

Conclusion

Appropriately designed SPIONs show promise for improving the treatment of skin-localized tumors through a 3-pronged effect: enhancing the immune response by increasing leukocyte infiltration, reducing the nutrient supply by decreasing its vascularity, and enhancing the penetration of chemotherapeutic drugs such as DOX and 5-FU through the skin. The application of such drugs transdermally offers a non-invasive treatment that ensures that the drugs reach their targets while reducing systemic toxicity. We anticipate that these SPIONs could improve the performance of other drugs in current use and enable drugs that had been previously ruled out due to systemic toxicity issues to be revisited.

Abbreviations

SC
stratum corneum; 5-FU:5-fluorouracil; DOX:doxorubicin; SPION:superparamagnetic iron oxide nanoparticle; RAFT:reversible addition-fragmentation chain-transfer; MAEP:monoacryloxyethyl phosphate; MPEG:poly(ethylene glycol) methyl ether; PEG:poly(ethylene glycol); DLS:dynamic light scattering; PBS:phosphate buffered saline; Rho-SPIONs:rhodamine-labelled SPIONs; PFA:paraformaldehyde; DAPI:4',6-diamidino-2-phenylindole; H&E:hematoxylin and eosin;

Declarations

Acknowledgements

The authors acknowledge the instruments and scientific and technical assistance, of Microscopy Australia at the Sydney Microscopy & Microanalysis, The University of Sydney.

Authors' contributions

Conceptualization: VR, BTTP, BSH, JGL; Data curation: VR; Formal analysis: VR, LFK, JGL; Funding acquisition: BSH; Investigation: VR, BTTP, NTHP, BJK, NP, NCD; Methodology: VR, JGL; Writing - Original Draft Preparation: VR; Writing – Review and Editing: All authors

Availability of data and materials

The datasets used and/or analyzed during the current study are available from the corresponding author on reasonable request.

Competing interests

BSH and BTTP are co-authors of patents for the synthesis and use of sterically stabilized nanoparticles: WO 2009/137890 and WO 2012/142669. SKJ holds shares in Zeta Therapeutics Pty Ltd, a company that could potentially benefit from the findings.

Consent for publication

Not applicable.

Ethics approval and consent to participate

All animal experiments were approved by the University of Sydney's Animal Ethics Committee (AEC 2015/744) and conducted in accordance with the Australian National Health and Medical Research Council guidelines and the Australian Code for the Care and Use of Animals for Scientific Purposes.

Funding

This study was funded by grants to JGL from the Australasian College of Dermatologists, and to BSH by Sirtex Australia Pty Ltd.

References

1. Ali A, Zafar H, Zia M, et al (2016) Synthesis, characterization, applications, and challenges of iron oxide nanoparticles. Nanotechnol Sci App 9:49–67. https://doi.org/10.2147/NSA.S99986
2. Alkilani AZ, McCrudden MTC, Donnelly RF (2015) Transdermal Drug Delivery: Innovative Pharmaceutical Developments Based on Disruption of the Barrier Properties of the stratum corneum. Pharmaceutics 7:438–470
3. Alvarez-Roman R, Merino G, Kalia YN, et al (2003) Skin permeability enhancement by low frequency sonophoresis: lipid extraction and transport pathways. J Pharm Sci 92:1138–46
4. Anandhakumar S, Raichur AM (2013) Polyelectrolyte/silver nanocomposite multilayer films as multifunctional thin film platforms for remote activated protein and drug delivery. Acta Biomater

9:8864–8874

5. Barenholz Y (2012) Doxil(R)–the first FDA-approved nano-drug: lessons learned. J Control Release 160:117–34
6. Baroli B, Ennas MG, Loffredo F, et al (2007) Penetration of Metallic Nanoparticles in Human Full-Thickness Skin. J Invest Dermatol 127:1701–1712. https://doi.org/10.1038/sj.jid.5700733
7. Bryce NS, Pham BTT, Fong NWS, et al (2013) The composition and end-group functionality of sterically stabilized nanoparticles enhances the effectiveness of co-administered cytotoxins. Biomater Sci 1:1260–1272. https://doi.org/10.1039/C3BM60120J
8. Carter P, Narasimhan B, Wang Q (2019) Biocompatible nanoparticles and vesicular systems in transdermal drug delivery for various skin diseases. Int J Pharm 555:49–62. https://doi.org/10.1016/j.ijpharm.2018.11.032
9. Cazares-Delgadillo J, Naik A, Ganem-Rondero A, et al (2007) Transdermal delivery of cytochrome C–A 12.4 kDa protein–across intact skin by constant-current iontophoresis. Pharm Res 24:1360–8
10. Chaudhuri P, Soni S, Sengupta S (2010) Single-walled carbon nanotube-conjugated chemotherapy exhibits increased therapeutic index in melanoma. Nanotechnology 21:025102
11. Chen G, Li D, Li J, et al (2015) Targeted doxorubicin delivery to hepatocarcinoma cells by lactobionic acid-modified laponite nanodisks. New J. Chem. 39:2847–2855
12. Dianzani C, Zara GP, Maina G, et al (2014) Drug delivery nanoparticles in skin cancers. Biomed Res Int 2014:895986
13. Eamegdool SS, Weible MW, Pham BTT, et al (2014) Ultrasmall superparamagnetic iron oxide nanoparticle prelabelling of human neural precursor cells. Biomaterials 35:5549–5564. https://doi.org/10.1016/j.biomaterials.2014.03.061
14. Fang J-Y, Hung C-F, Fang Y-P, Chan T-F (2004) Transdermal iontophoresis of 5-fluorouracil combined with electroporation and laser treatment. Int J Pharm 270:241–249
15. Fernandes R, Smyth NR, Muskens OL, et al (2015) Interactions of Skin with Gold Nanoparticles of Different Surface Charge, Shape, and Functionality. Small 11:713–721
16. Galluzzi L, Buqué A, Kepp O, et al (2015) Immunological Effects of Conventional Chemotherapy and Targeted Anticancer Agents. Cancer Cell 28:690–714. https://doi.org/10.1016/j.ccell.2015.10.012
17. Garbe C, Eigentler TK, Keilholz U, et al (2011) Systematic review of medical treatment in melanoma: current status and future prospects. Oncologist 16:5–24
18. Gautam A, Nanda JS, Samuel JS, et al (2016) Topical Delivery of Protein and Peptide Using Novel Cell Penetrating Peptide IMT-P8. Sci. Rep. 6:26278
19. Hansen S, Lehr C-M (2012) Nanoparticles for transcutaneous vaccination. Microb. Biotechnol. 5:156–167
20. Hasany S, Rehman A, Ahmed I, Rajan J (2012) Systematic review of the preparation techniques of iron oxide magnetic nanoparticles. Nanosci Nanotechnol 2(6):148–158

21. Herndon TO, Gonzalez S, Gowrishankar TR, et al (2004) Transdermal microconduits by microscission for drug delivery and sample acquisition. BMC Med 2:12
22. Hsiao PF, Peng S, Tang TC, et al (2016) Enhancing the in vivo transdermal delivery of gold nanoparticles using poly(ethylene glycol) and its oleylamine conjugate. Int J Nanomedicine 11:1867–78
23. Jain N, Wang Y, Jones SK, et al (2010) Optimized steric stabilization of aqueous ferrofluids and magnetic nanoparticles. Langmuir 26:4465–72
24. Kievit FM, Wang FY, Fang C, et al (2011) Doxorubicin loaded iron oxide nanoparticles overcome multidrug resistance in cancer in vitro. J. Controlled Release 152:76–83
25. Kotiyan P, Majali A., Vavia P, Bhardwaj Y, Sabarwal S A (2004) Electronbeam irradiation: a novel technology for the development oftransdermal system of isosorbide dinitrate. Int J Pharm 270 (1)
26. Lohade AA, Jain RR, Iyer K, et al (2016) A Novel Folate-Targeted Nanoliposomal System of Doxorubicin for Cancer Targeting. AAPS PharmSciTech 17:1298–1311. https://doi.org/10.1208/s12249-015-0462-2
27. Lombry C, Dujardin N, Preat V (2000) Transdermal delivery of macromolecules using skin electroporation. Pharm Res 17:32–7
28. Lv Q, He C, Quan F, et al (2017) DOX/IL-2/IFN-γ co-loaded thermo-sensitive polypeptide hydrogel for efficient melanoma treatment. Bioact. Mater. 3:118–128
29. Massart R, Dubois E, Cabuil V, Hasmonay E (1995) Preparation and Properties of Monodisperse Magnetic Fluids. J. Magn. Magn. Mater. 149:1–5
30. Matsui T, Amagai M (2015) Dissecting the formation, structure and barrier function of the stratum corneum. Int Immunol 27:269–280. https://doi.org/10.1093/intimm/dxv013
31. Mulens-Arias V, Rojas JM, Sanz-Ortega L, et al (2019) Polyethylenimine-coated superparamagnetic iron oxide nanoparticles impair in vitro and in vivo angiogenesis. Nanomedicine Nanotechnol Biol Med 21:102063. https://doi.org/10.1016/j.nano.2019.102063
32. Mundra V, Li W, Mahato RI (2015) Nanoparticle-mediated drug delivery for treating melanoma. Nanomed. 10:2613–2633
33. Murthy SN, Sammeta SM, Bowers C (2010) Magnetophoresis for enhancing transdermal drug delivery: Mechanistic studies and patch design. J Control Release 148:197–203
34. Nose K, Pissuwan D, Goto M, et al (2012) Gold nanorods in an oil-base formulation for transdermal treatment of type 1 diabetes in mice. Nanoscale 4:3776–80
35. Oh JM, Park DH, Choi SJ, Choy JH (2012) LDH nanocontainers as bio-reservoirs and drug delivery carriers. Recent Pat Nanotechnol 6:200–17
36. Ozcan A, Sahin D, Impellizzieri D, et al (2020) Nanoparticle-Coupled Topical Methotrexate Can Normalize Immune Responses and Induce Tissue Remodeling in Psoriasis. J Invest Dermatol 140:1003-1014 e8

37. Palanisamy S, Wang YM (2019) Superparamagnetic iron oxide nanoparticulate system: synthesis, targeting, drug delivery and therapy in cancer. Dalton Trans 48:9490–9515
38. Palmer BC, DeLouise LA (2016) Nanoparticle-Enabled Transdermal Drug Delivery Systems for Enhanced Dose Control and Tissue Targeting. Molecules 21:1719. https://doi.org/10.3390/molecules21121719
39. Pan J, Rostamizadeh K, Filipczak N, Torchilin VP (2019) Polymeric Co-Delivery Systems in Cancer Treatment: An Overview on Component Drugs' Dosage Ratio Effect. Mol. Basel Switz. 24:1035
40. Pelaz B, Alexiou C, Alvarez-Puebla RA, et al (2017) Diverse Applications of Nanomedicine. ACS Nano 11:2313–2381. https://doi.org/10.1021/acsnano.6b06040
41. Pham BT, Jain N, Kuchel PW, et al (2015) The interaction of sterically stabilized magnetic nanoparticles with fresh human red blood cells. In: Int. J. Nanomedicine. https://www.dovepress.com/the-interaction-of-sterically-stabilized-magnetic-nanoparticles-with-f-peer-reviewed-article-IJN. Accessed 15 Jun 2020
42. Pham BTT, Colvin EK, Pham NTH, et al (2018) Biodistribution and Clearance of Stable Superparamagnetic Maghemite Iron Oxide Nanoparticles in Mice Following Intraperitoneal Administration. Int J Mol Sci 19
43. Pham TN, Lengkeek NA, Greguric I, et al (2017) Tunable and noncytotoxic PET/SPECT-MRI multimodality imaging probes using colloidally stable ligand-free superparamagnetic iron oxide nanoparticles. Int J Nanomedicine 12:899–909. https://doi.org/10.2147/IJN.S127171
44. Prausnitz MR (2004) Microneedles for transdermal drug delivery. Adv Drug Deliv Rev 56:581–7
45. Prausnitz MR, Langer R (2008) Transdermal drug delivery. Nat Biotechnol 26:1261–8. https://doi.org/10.1038/nbt.1504
46. Rao Y, Chen W, Liang X, et al (2015) Epirubicin-Loaded Superparamagnetic Iron-Oxide Nanoparticles for Transdermal Delivery: Cancer Therapy by Circumventing the Skin Barrier. Small 11:239–247. https://doi.org/10.1002/smll.201400775
47. Rosenberg SA, Yannelli JR, Yang JC, et al (1994) Treatment of Patients With Metastatic Melanoma With Autologous Tumor-Infiltrating Lymphocytes and Interleukin 2. JNCI J. Natl. Cancer Inst. 86:1159–1166
48. Ruifrok A, Johnston D (2001) Ruifrok AC, Johnston DA. Quantification of histochemical staining by color deconvolution. Anal Quant Cytol Histol 23: 291-299. Anal Quant Cytol Histol Int Acad Cytol Am Soc Cytol 23:291–9
49. Santini B, Zanoni I, Marzi R, et al (2015) Cream formulation impact on topical administration of engineered colloidal nanoparticles. PLoS One 10:e0126366
50. Sheth RA, Wen X, Li J, et al (2020) Doxorubicin-loaded hollow gold nanospheres for dual photothermal ablation and chemoembolization therapy. Cancer Nanotechnol 11:6. https://doi.org/10.1186/s12645-020-00062-8
51. Shubayev VI, Pisanic TR, Jin S (2009) Magnetic nanoparticles for theragnostics. Adv. Drug Deliv. Rev. 61:467–477

52. Tang J-Q, Hou X-Y, Yang C-S, et al (2017) Recent developments in nanomedicine for melanoma treatment. Int J Cancer 141:646–653. https://doi.org/10.1002/ijc.30708
53. Tomayko MM, Reynolds CP (1989) Determination of subcutaneous tumor size in athymic (nude) mice. Cancer Chemother Pharmacol 24:148–154. https://doi.org/10.1007/BF00300234
54. Vanella V, Festino L, Trojaniello C, et al (2019) The Role of BRAF-Targeted Therapy for Advanced Melanoma in the Immunotherapy Era. Curr Oncol Rep 21:76. https://doi.org/10.1007/s11912-019-0827-x
55. Vannucci L, Falvo E, Fornara M, et al (2012) Selective targeting of melanoma by PEG-masked protein-based multifunctional nanoparticles. Int J Nanomedicine 7:1489–509
56. Veiseh O, Gunn JW, Zhang M (2010) Design and fabrication of magnetic nanoparticles for targeted drug delivery and imaging. Adv. Drug Deliv. Rev. 62:284–304
57. Wang F, Wang YC, Dou S, et al (2011) Doxorubicin-tethered responsive gold nanoparticles facilitate intracellular drug delivery for overcoming multidrug resistance in cancer cells. ACS Nano 5:3679–92
58. Wang M, Marepally SK, Vemula PK, Xu C (2016) Chapter 5 - Inorganic Nanoparticles for Transdermal Drug Delivery and Topical Application. Nanosci. Dermatol. 57–72
59. Weiss RB (1992) The anthracyclines: will we ever find a better doxorubicin? Semin Oncol 19:670–86
60. Yu M, Jambhrunkar S, Thorn P, et al (2013) Hyaluronic acid modified mesoporous silica nanoparticles for targeted drug delivery to CD44-overexpressing cancer cells. Nanoscale 5:178–83
61. Zvyagin AV, Zhao X, Gierden A, et al (2008) Imaging of zinc oxide nanoparticle penetration in human skin in vitro and in vivo. J Biomed Opt 13:064031

Figures

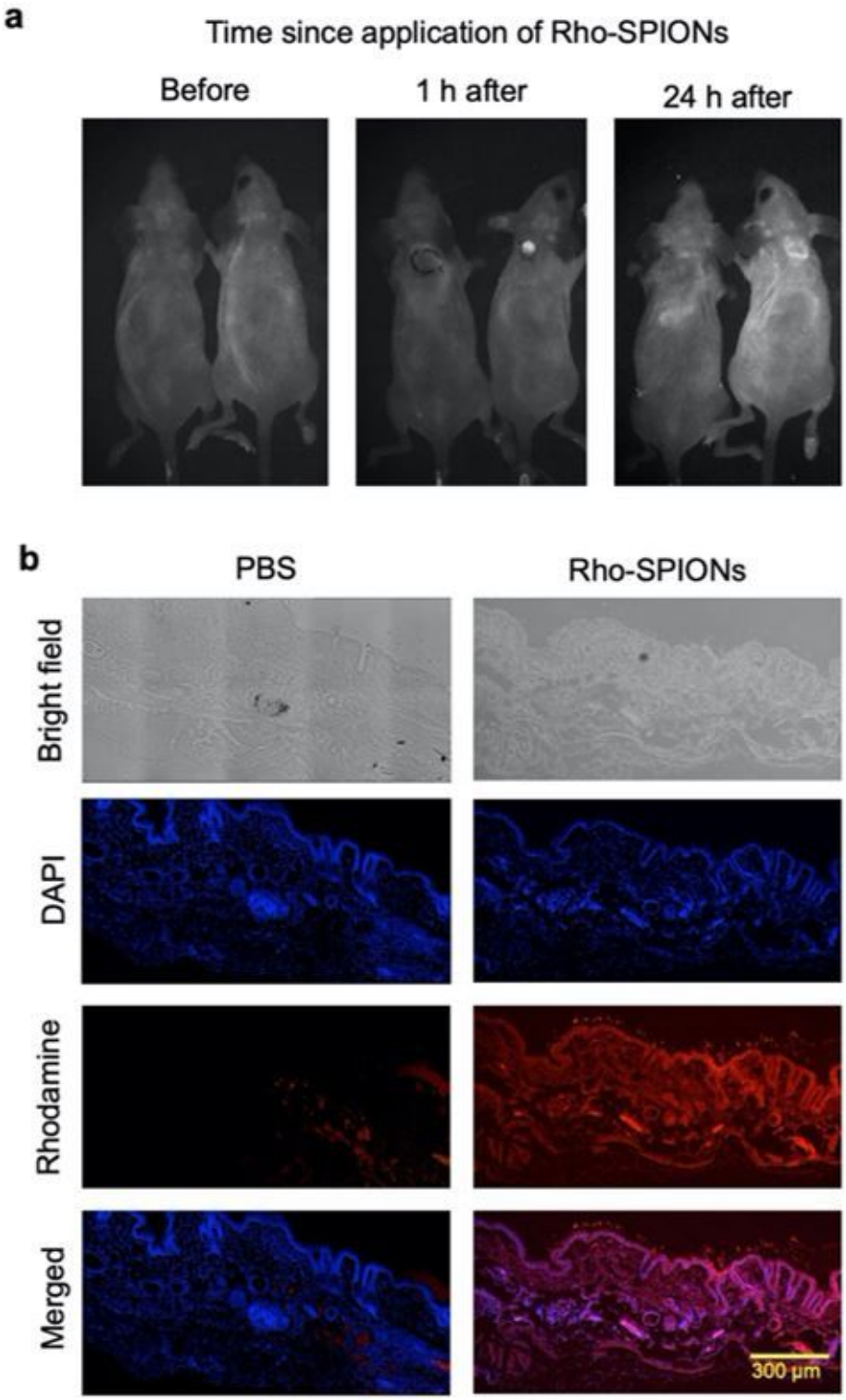

Figure 1

Rhodamine labelled SPIONs penetrate mouse skin. To examine the penetration of topically applied SPIONs into the skin, rhodamine labelled SPIONs (2 mg/mL in 20 µL PBS, mouse on the right) or vehicle (20 µL, mouse on the left) were applied to the back skin of mice. One hour after application, unabsorbed solution was removed by wiping. a. Mouse whole-body fluorescence images were acquired at the time points indicated. b. Fluorescence micrographs of frozen fixed sections of the Rho-SPION-treated area of

skin, 24 hours after application, showing brightfield, nuclear counterstain (DAPI) and rhodamine signals. Representative images of 1-2 mice and experiment repeated 3 times.

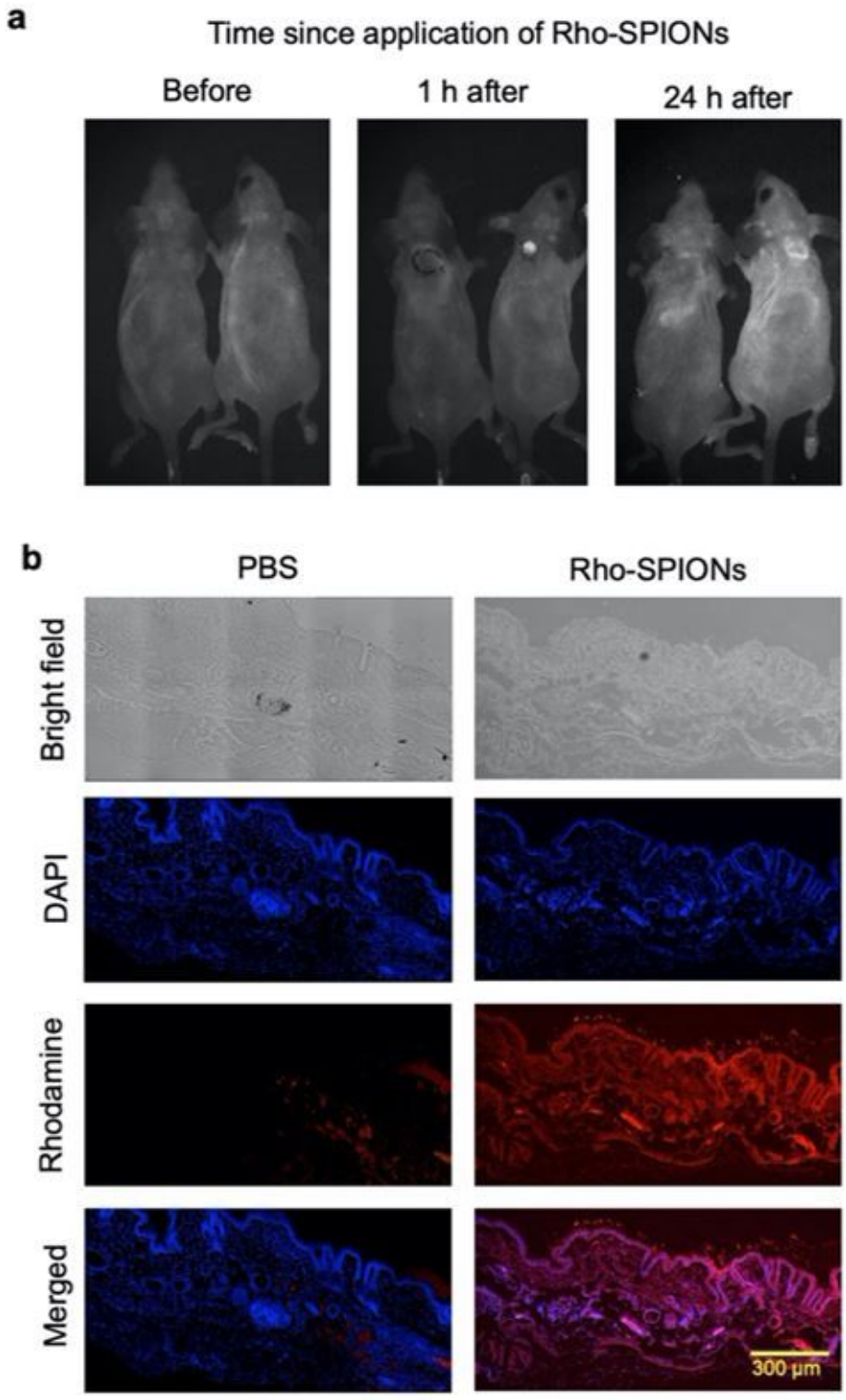

Figure 1

Rhodamine labelled SPIONs penetrate mouse skin. To examine the penetration of topically applied SPIONs into the skin, rhodamine labelled SPIONs (2 mg/mL in 20 µL PBS, mouse on the right) or vehicle (20 µL, mouse on the left) were applied to the back skin of mice. One hour after application, unabsorbed

solution was removed by wiping. a. Mouse whole-body fluorescence images were acquired at the time points indicated. b. Fluorescence micrographs of frozen fixed sections of the Rho-SPION-treated area of skin, 24 hours after application, showing brightfield, nuclear counterstain (DAPI) and rhodamine signals. Representative images of 1-2 mice and experiment repeated 3 times.

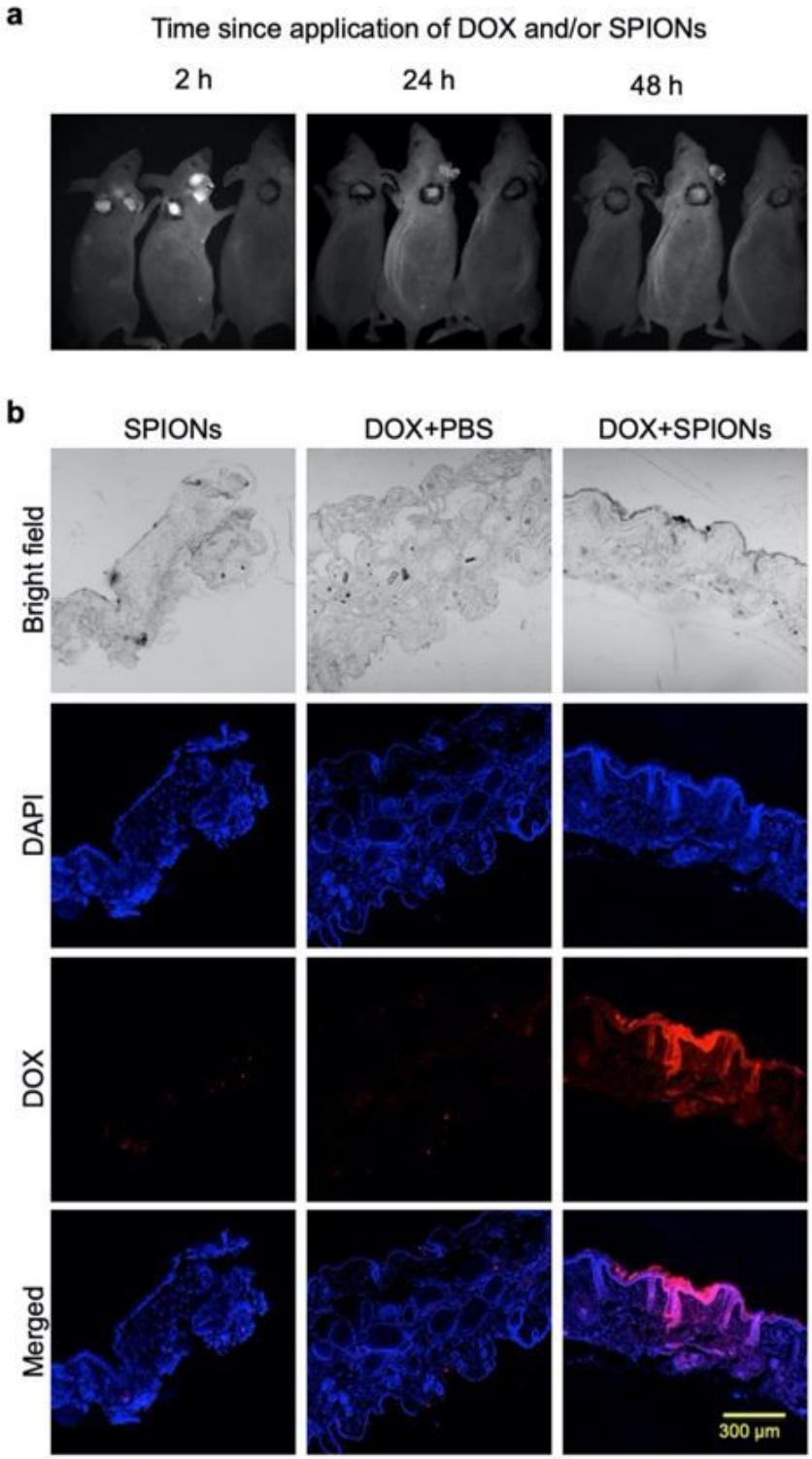

Figure 2

SPIONs improve the penetration of DOX into mouse skin. a. Unlabelled SPIONs alone (mouse on right), DOX alone (mouse in middle) or unlabelled SPIONs plus DOX (mouse on left) were applied topically to the back skin and right ear of mice. After 2 hours, unabsorbed particles and DOX solution were removed by wiping. Mouse whole-body fluorescence images were acquired at the indicated time points after application. b. Fluorescence micrographs of frozen sections of the treated area of skin, fixed 48 hours after application, showing brightfield, nuclear counterstain (DAPI) and DOX channel images. Representative images of an experiment repeated 3 times.

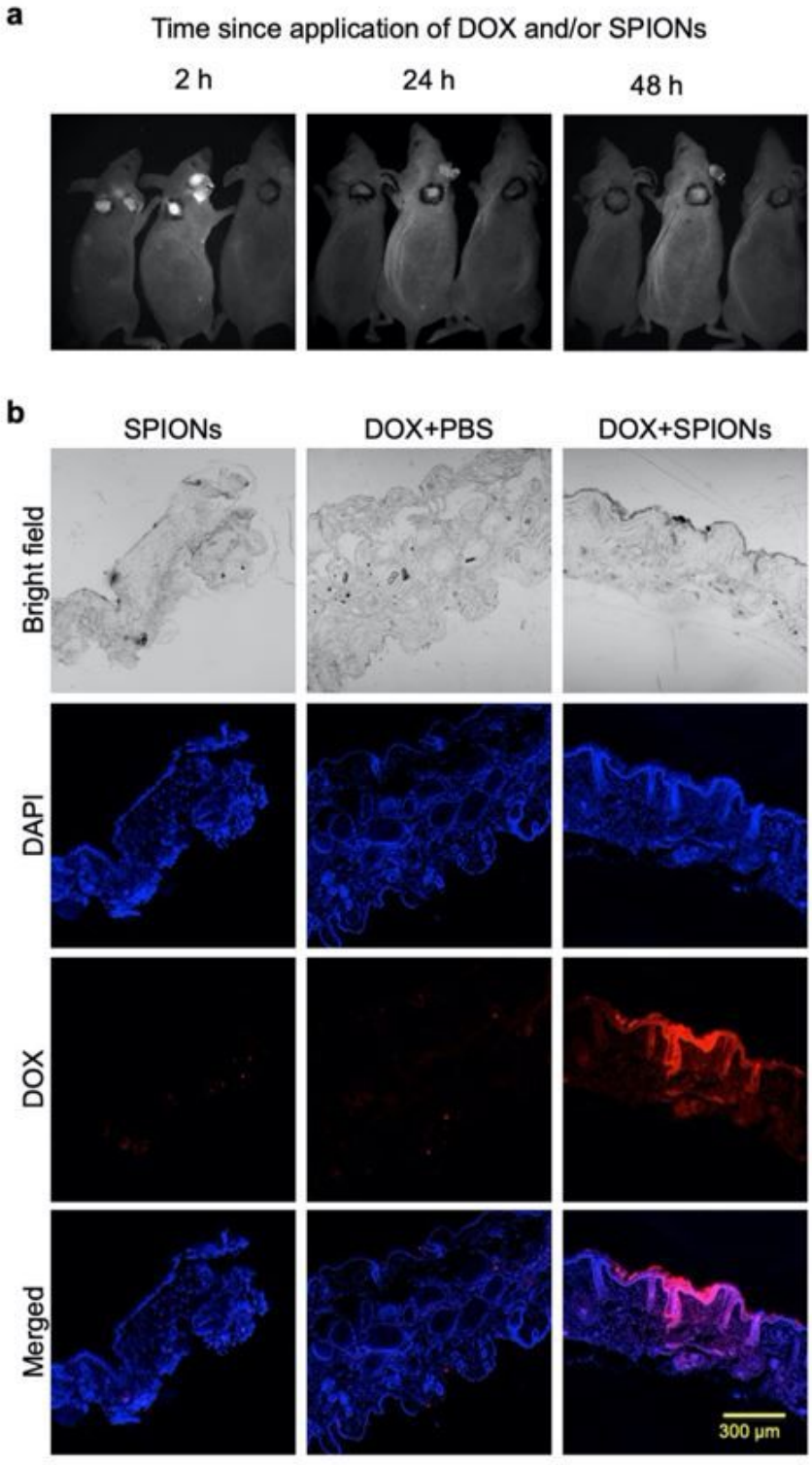

Figure 2

SPIONs improve the penetration of DOX into mouse skin. a. Unlabelled SPIONs alone (mouse on right), DOX alone (mouse in middle) or unlabelled SPIONs plus DOX (mouse on left) were applied topically to the back skin and right ear of mice. After 2 hours, unabsorbed particles and DOX solution were removed by wiping. Mouse whole-body fluorescence images were acquired at the indicated time points after application. b. Fluorescence micrographs of frozen sections of the treated area of skin, fixed 48 hours after application, showing brightfield, nuclear counterstain (DAPI) and DOX channel images. Representative images of an experiment repeated 3 times.

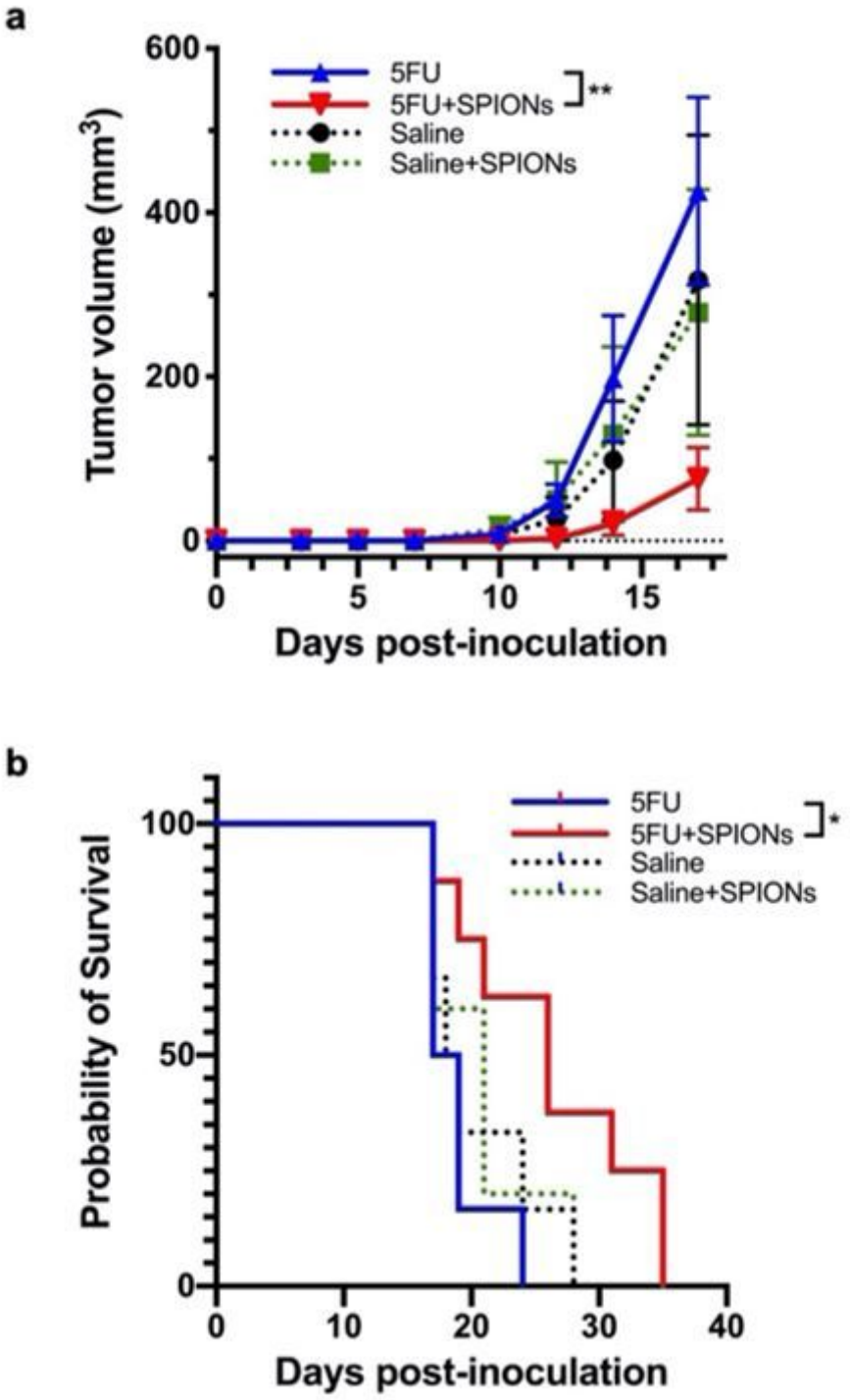

Figure 3

Co-application of topical 5-FU and SPIONs reduces mouse melanoma tumor growth. Melanoma tumors in 8 week old hairless mice were initiated by subcutaneous injection of 1 x104 B16F10-tdTomato mouse melanoma cells on the back of the mouse. Three days post cell injection, mice were treated with topical application at the tumor site of 60µL of either saline alone, SPIONs alone, 5-FU (1 mM) alone or 5-FU plus SPIONs (1 mg/mL) three times a week (n = 5-8 mice per group). a. Tumor size. ** P< 0.01, repeated

measures ANOVA. b. Survival, in terms of the time taken for the tumor to reach 10mm diameter. *P< 0.05, log-rank (Mantel-Cox) test.

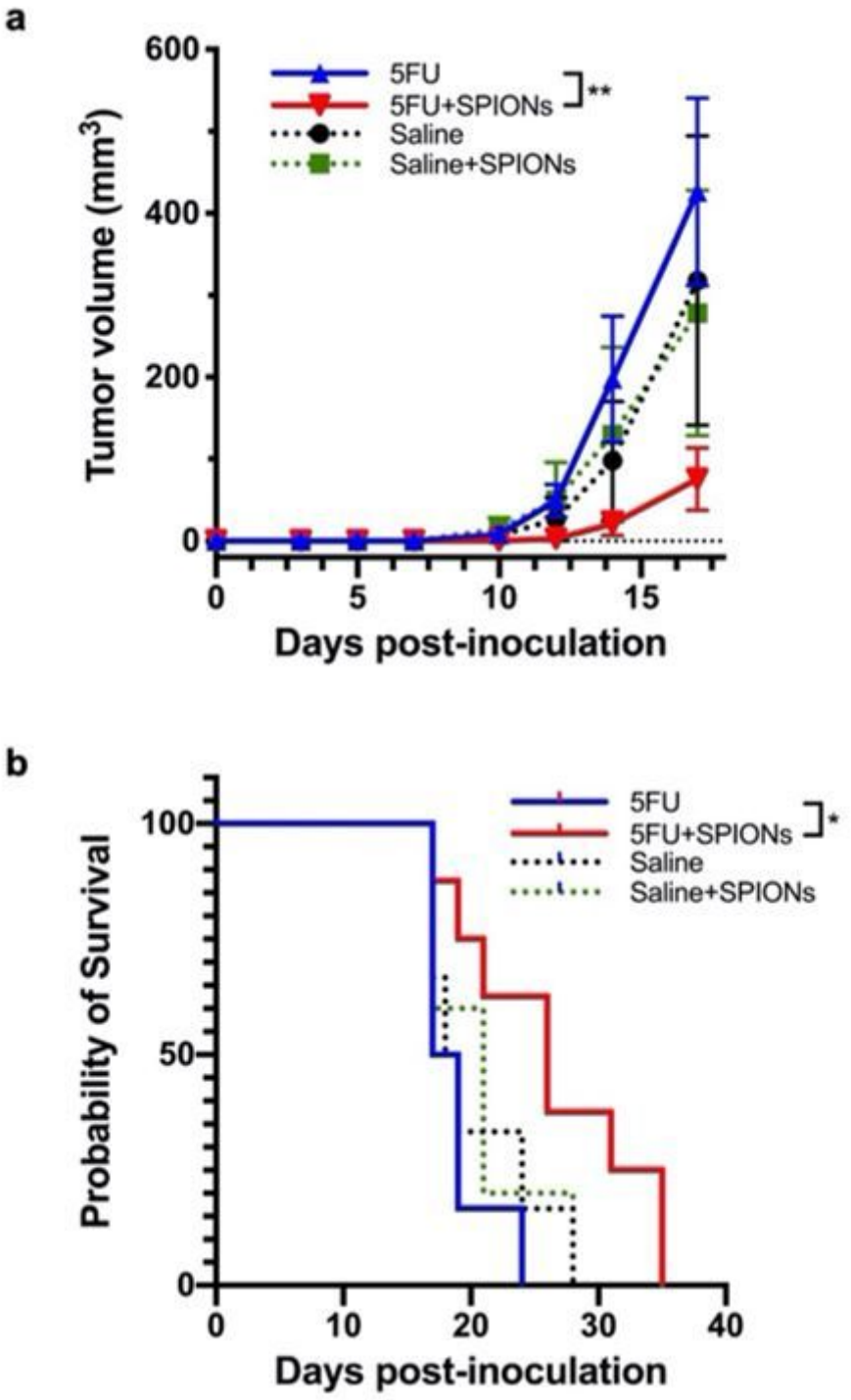

Figure 3

Co-application of topical 5-FU and SPIONs reduces mouse melanoma tumor growth. Melanoma tumors in 8 week old hairless mice were initiated by subcutaneous injection of 1 x104 B16F10-tdTomato mouse melanoma cells on the back of the mouse. Three days post cell injection, mice were treated with topical

application at the tumor site of 60μL of either saline alone, SPIONs alone, 5-FU (1 mM) alone or 5-FU plus SPIONs (1 mg/mL) three times a week (n = 5-8 mice per group). a. Tumor size. ** P< 0.01, repeated measures ANOVA. b. Survival, in terms of the time taken for the tumor to reach 10mm diameter. *P< 0.05, log-rank (Mantel-Cox) test.

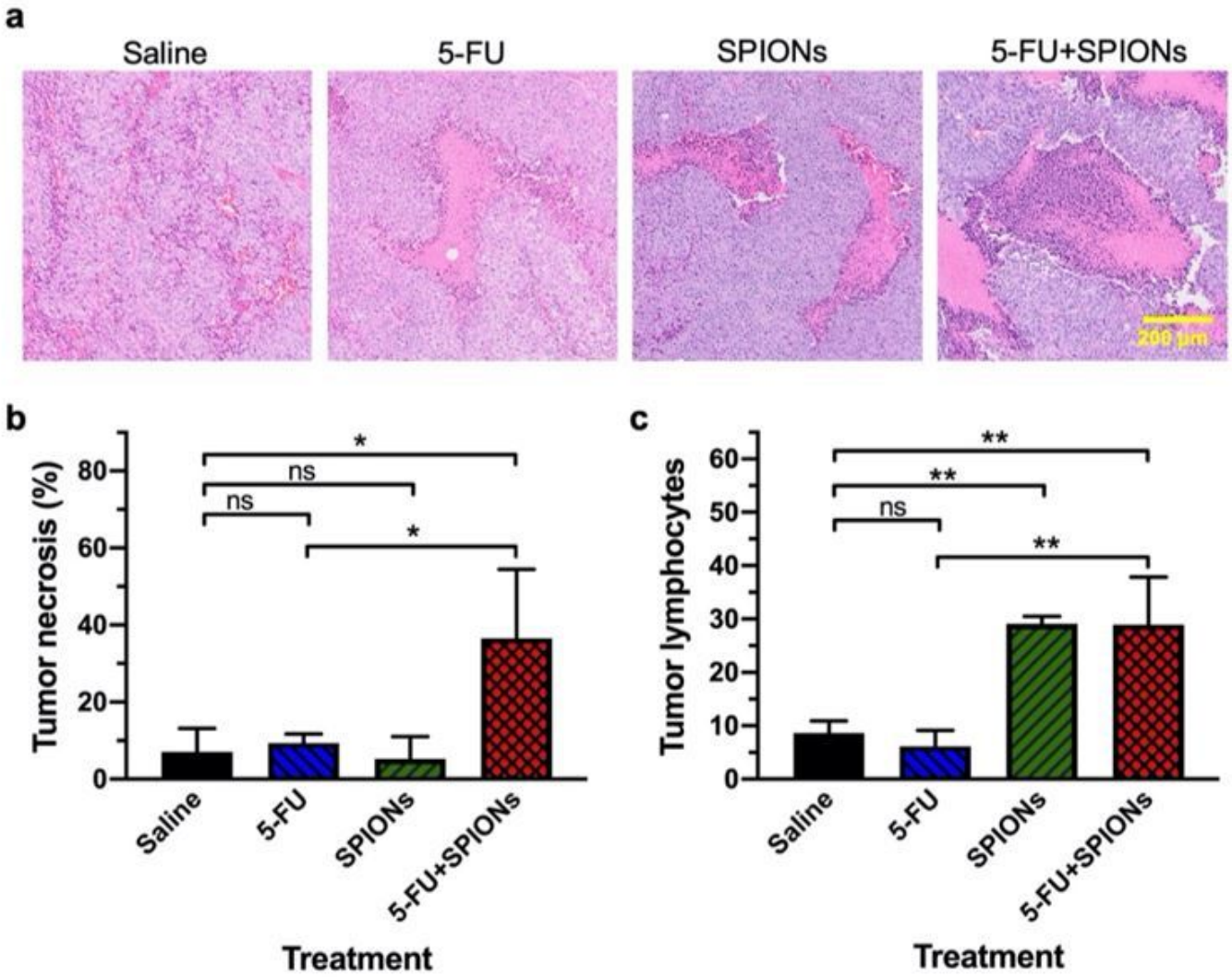

Figure 4

Co-treatment of 5-FU with SPIONs increases necrosis and tumor infiltrating lymphocytes in melanoma tumors. a. Representative images of hematoxylin and eosin stained sections of B16F10- tdTomato melanoma tumors that had been treated topically with either vehicle (saline), 5-FU alone, SPIONs alone or both 5-FU and SPIONs. b. The extent of necrosis in the tumors. c. The number of infiltrating lymphocytes per 1.3mm2 field in the tumors. The data are shown as the mean ± standard deviation of n = 3 mice per group. One-way ANOVA with Sidak's multiple comparisons adjustment indicating significant difference at *p < 0.05 and **p < 0.01.

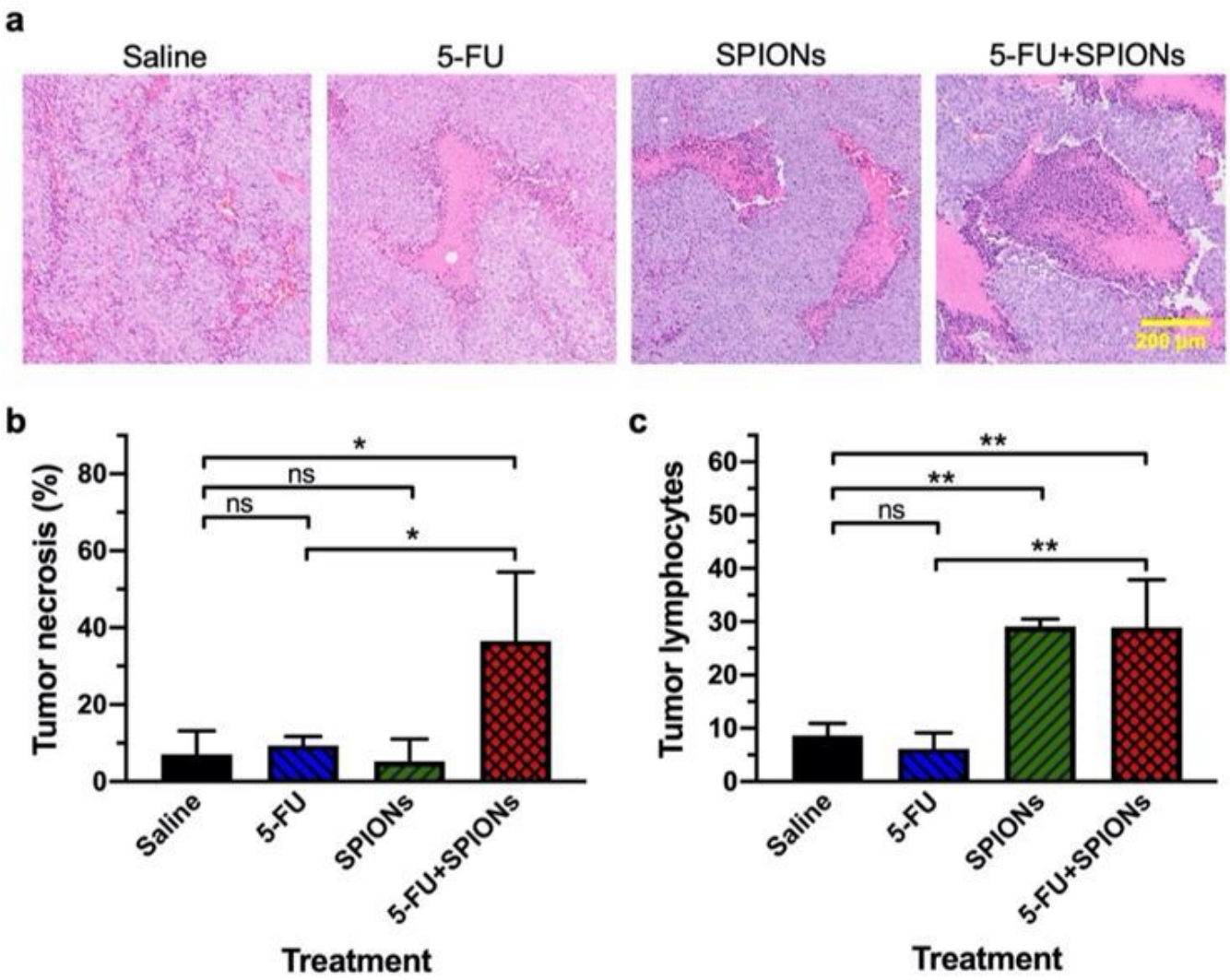

Figure 4

Co-treatment of 5-FU with SPIONs increases necrosis and tumor infiltrating lymphocytes in melanoma tumors. a. Representative images of hematoxylin and eosin stained sections of B16F10- tdTomato melanoma tumors that had been treated topically with either vehicle (saline), 5-FU alone, SPIONs alone or both 5-FU and SPIONs. b. The extent of necrosis in the tumors. c. The number of infiltrating lymphocytes per 1.3mm2 field in the tumors. The data are shown as the mean ± standard deviation of n = 3 mice per group. One-way ANOVA with Sidak's multiple comparisons adjustment indicating significant difference at *$p < 0.05$ and **$p < 0.01$.

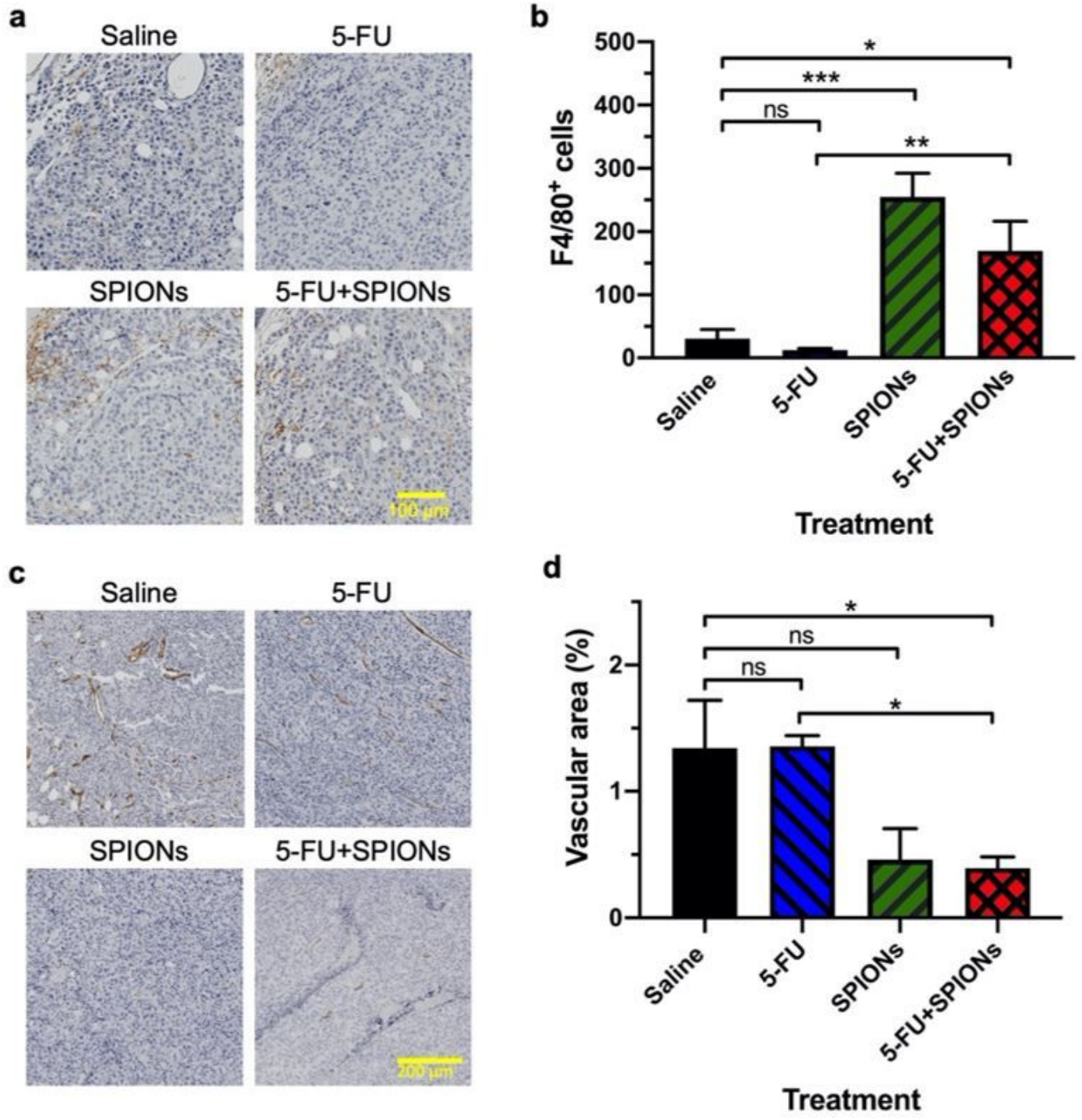

Figure 5

Co-administration of SPIONs with 5-FU increases macrophage infiltration and inhibits blood vessel formation in tumors. a. Representative images of B16F10-tdTomato melanoma tumors treated topically with either vehicle (Saline), 5-FU alone, SPIONs alone or both 5-FU and SPIONs. Sections were stained for macrophages with anti-F4/80 antibody (brown). b. Quantification of tumor-infiltrating macrophages from F4/80 immunostained sections. c. Representative images of melanoma tumors treated topically with vehicle (Saline) 5-FU, SPIONs or both 5-FU and SPIONs. Sections were stained for endothelial cells with

anti-CD31 antibody. The data are shown as the mean ± SEM of n=5 measurements from 2 mice per group. d. Quantification of vascularization from CD31-immunostained sections. One-way ANOVA followed by Sidak's multiple comparisons adjustment indicating significant difference at *p < 0.05, **p < 0.01 and *** p < 0.001.

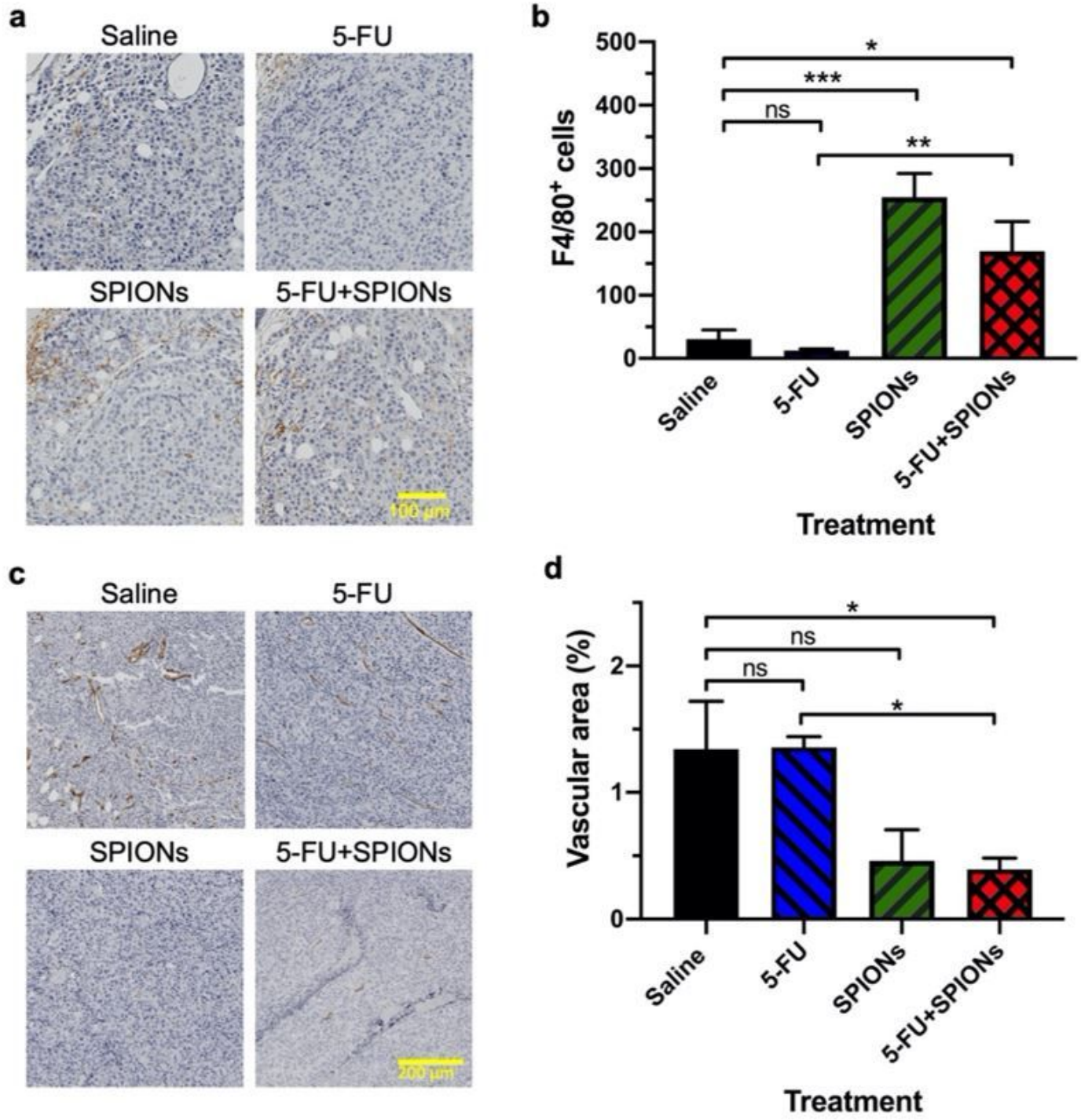

Figure 5

Co-administration of SPIONs with 5-FU increases macrophage infiltration and inhibits blood vessel formation in tumors. a. Representative images of B16F10-tdTomato melanoma tumors treated topically

with either vehicle (Saline), 5-FU alone, SPIONs alone or both 5-FU and SPIONs. Sections were stained for macrophages with anti-F4/80 antibody (brown). b. Quantification of tumor-infiltrating macrophages from F4/80 immunostained sections. c. Representative images of melanoma tumors treated topically with vehicle (Saline) 5-FU, SPIONs or both 5-FU and SPIONs. Sections were stained for endothelial cells with anti-CD31 antibody. The data are shown as the mean ± SEM of n=5 measurements from 2 mice per group. d. Quantification of vascularization from CD31-immunostained sections. One-way ANOVA followed by Sidak's multiple comparisons adjustment indicating significant difference at *p < 0.05, **p < 0.01 and *** p < 0.001.

Supplementary Files

This is a list of supplementary files associated with this preprint. Click to download.

- Supplementarydata20201129.pdf
- Supplementarydata20201129.pdf